Guanine Nucleotide Exchange Factor Vav1 Regulates Perivascular Homing and Bone Marrow Retention of Hematopoietic Stem and Progenitor Cells

Guanine nucleotide exchange factor Vav1 regulates perivascular homing and bone marrow retention of hematopoietic stem and progenitor cells

Abel Sanchez-Aguilera[a], Yun-Jung Lee[b], Cristina Lo Celso[c,d], Francesca Ferraro[c,d], Kristina Brumme[a], Subhanjan Mondal[e,f], Chaekyun Kim[a,g], Adrienne Dorrance[a], Hongbo R. Luo[e,f], David T. Scadden[c,d,h], and David A. Williams[a,c,1]

[a]Division of Hematology/Oncology, Children's Hospital Boston and Dana-Farber Cancer Institute, Boston, MA 02115; [b]Department of Pathology and Laboratory Medicine, University of Cincinnati, Cincinnati, OH 45267; [c]Harvard Stem Cell Institute, Cambridge, MA 02138; [d]Center for Regenerative Medicine, Massachusetts General Hospital, Boston, MA 02114; [e]Department of Pathology, Harvard Medical School and Dana-Farber/Harvard Cancer Center, Boston, MA 02115; [f]Department of Laboratory Medicine, Children's Hospital Boston, Boston, MA 02115; [g]Inha University School of Medicine, Incheon 400-712, Korea; and [h]Department of Stem Cell and Regenerative Biology, Harvard University, Cambridge, MA 02138

Edited* by Joan S. Brugge, Harvard Medical School, Boston, MA, and approved May 2, 2011 (received for review February 4, 2011)

Engraftment and maintenance of hematopoietic stem and progenitor cells (HSPC) depend on their ability to respond to extracellular signals from the bone marrow microenvironment, but the critical intracellular pathways integrating these signals remain poorly understood. Furthermore, recent studies provide contradictory evidence of the roles of vascular versus osteoblastic niche components in HSPC function. To address these questions and to dissect the complex upstream regulation of Rac GTPase activity in HSPC, we investigated the role of the hematopoietic-specific guanine nucleotide exchange factor Vav1 in HSPC localization and engraftment. Using intravital microscopy assays, we demonstrated that transplanted *Vav1*$^{-/-}$ HSPC showed impaired early localization near nestin^{+} perivascular mesenchymal stem cells; only 6.25% of *Vav1*$^{-/-}$ HSPC versus 45.8% of wild-type HSPC were located less than 30 μm from a nestin^{+} cell. Abnormal perivascular localization correlated with decreased retention of *Vav1*$^{-/-}$ HSPC in the bone marrow (44–60% reduction at 48 h posttransplant, compared with wild-type) and a very significant defect in short- and long-term engraftment in competitive and noncompetitive repopulation assays (<1.5% chimerism of *Vav1*$^{-/-}$ cells vs. 53–63% for wild-type cells). The engraftment defect of *Vav1*$^{-/-}$ HSPC was not related to alterations in proliferation, survival, or integrin-mediated adhesion. However, *Vav1*$^{-/-}$ HSPC showed impaired responses to SDF1α, including reduced in vitro migration in time-lapse microscopy assays, decreased circadian and pharmacologically induced mobilization in vivo, and dysregulated Rac/Cdc42 activation. These data suggest that Vav1 activity is required specifically for SDF1α-dependent perivascular homing of HSPC and suggest a critical role for this localization in retention and subsequent engraftment.

Hematopoietic stem cells (HSC) are defined by their ability to self-renew and the potential to generate all mature hematopoietic lineages, both during homeostasis and after transplantation. Maintenance of these functions critically depends on the interaction of HSC with one or several specialized microenvironments (so-called niches) in the bone marrow (BM) (1). Different cell populations have been proposed to form niches for HSC, including osteoblasts (2, 3), endothelial cells (4), stromal-derived factor-1 alpha (SDF1α)-expressing reticular cells (5), and nestin^{+} mesenchymal stem cells (MSC) (6). These components appear to be spatially related in the BM (5–7), but it is not clear whether they constitute a number of functionally distinct HSC niches or contribute to a complex multicellular hematopoietic microenvironment, and, specifically, there is conflicting evidence on the relative roles of osteoblastic versus vascular components of the niche in regulating hematopoietic stem and progenitor cell (HSPC) functions. Extracellular cues proposed to play a decisive role in hematopoietic stem/progenitor cell interaction with and retention in the niche include stem cell factor (SCF), concentration gradients of the chemoattractant CXCL12/SDF1α, and β_1 integrin-mediated adhesion to extracellular matrix and VCAM1^{+} endothelium (8–12).

The crucial intracellular pathways triggered by these signals are less well characterized, and how they are coordinated to regulate HSPC localization relative to different components of the niche is not known. Although previous work has provided insight into the role of Rho GTPases Rac1, Rac2 (13, 14), and Cdc42 (15) in HSPC trafficking and engraftment (reviewed in ref. 16), cells deficient in these GTPases show multiple proliferative, survival, and cytoskeletal defects, which precluded a more precise dissection of the key pathways regulating HSPC trafficking and localization. Thus, Rac-deficient HSPC show reduced chemotaxis to SDF1α and β_1 integrin-mediated adhesion in vitro but also defects in SCF-mediated proliferation and survival (14), consistent with the integration of multiple receptors and signaling pathways. In vivo, Rac1 is required for HSPC engraftment and endosteal localization in the BM, whereas deletion of both Rac1 and Rac2 not only impairs engraftment but causes massive HSPC mobilization (13, 14). Dissecting this complex regulation involves defining the functional interactions between GTPases and specific guanine nucleotide exchange factors (GEFs) that activate them (17), and this remains a major challenge.

Here we focus on the Vav subfamily of GEFs, which consists of three related proteins: Vav1 (hematopoietic-specific) and Vav2 and Vav3 (more broadly expressed) (18). Vav proteins have nonredundant functions in lymphopoiesis related to their role in immunoreceptor signaling. Thus, *Vav1*$^{-/-}$ mice show defective T and B-1 cell development (19–21), whereas mutation of all three Vav genes completely impairs both the B- and T-lymphoid lineages (22). In neutrophils, Vav proteins are required for sustained β_2 integrin-mediated adhesion, intravascular endothelial crawling, and superoxide production (23–25). Despite the well-characterized function of Vav proteins in immune processes, virtually nothing is known about the role of these GEFs in primitive hematopoietic cells. We hypothesized that the hematopoietic-specific GEF Vav1 may regulate HSPC engraftment and retention by mediating responses to a subset of microenvironmental signals.

Author contributions: A.S.-A., H.R.L., D.T.S., and D.A.W. designed research; A.S.-A., Y.-J.L., C.L.C., F.F., K.B., S.M., C.K., A.D., H.R.L., and D.T.S. performed research; A.S.-A., Y.-J.L., C.L.C., F.F., S.M., C.K., and D.A.W. analyzed data; and A.S.-A. and D.A.W. wrote the paper.

The authors declare no conflict of interest.

*This Direct Submission article had a prearranged editor.

[1]To whom correspondence should be addressed. E-mail: dawilliams@childrens.harvard.edu.

This article contains supporting information online at www.pnas.org/lookup/suppl/doi:10.1073/pnas.1102018108/-/DCSupplemental.

Therefore, we investigated the effect of genetic deletion of Vav1 on HSPC homing, localization, and retention in the BM microenvironment, and the role of Vav1 in mediating HSPC responses to chemokine and adhesion ligands. Our results suggest that Vav1 activity is required specifically for SDF1α-dependent perivascular homing of HSPC and suggest a critical role for this localization in BM retention and subsequent engraftment.

Results

Dysregulated Rho GTPase Activation in *Vav1*$^{-/-}$ Hematopoietic Progenitors. We reasoned that, if Vav1 is a biologically relevant and nonredundant GEF in HSPC, deletion of Vav1 in this cellular compartment would induce alterations in Rho GTPase activation. In addition, Vav1 itself would be expected to be activated by factors present in the BM microenvironment. Vav1 was rapidly phosphorylated in WT hematopoietic progenitors in response to in vitro stimulation by SCF/SDF1α (Fig. 1*A Upper*). Whereas *Vav1*$^{-/-}$ cells did not show any agonist-induced tyrosine phosphorylation, a cross-reactive band was observed in nonstimulated *Vav1*$^{-/-}$ cells. As Vav1 protein was absent from *Vav1*$^{-/-}$ immunoprecipitates (Fig. 1*A Lower*), this suggested a compensatory, abnormal increase in the activation of another Vav protein. Indeed, increased baseline phosphorylation of Vav3 was detected with a phosphospecific antibody in *Vav1*$^{-/-}$ progenitors (Fig. 1*B*).

We observed two distinct abnormalities in hematopoietic progenitors isolated from the BM of *Vav1*$^{-/-}$ mice. First, the baseline levels of GTP-bound (active) Rac and Cdc42 were unexpectedly elevated, which is consistent with the dysregulated activation of either or both Vav2 and Vav3. The total level of Rac and Cdc42 proteins was also increased, compared with WT progenitors (Fig. 1*C*). Second, in the absence of Vav1, both Rac and Cdc42 were unresponsive to in vitro stimulation by the combination of SCF and SDF1α, known critical regulators of HSPC engraftment and activators of Rac and Cdc42 GTPases in HSPC (13–15) (Fig. 1*C*). To determine whether these changes were physiologically relevant, we studied known downstream targets of Rac which we have previously demonstrated to be involved in HSPC homing and retention (13, 14, 26, 27). *Vav1*$^{-/-}$ progenitors showed increased baseline activation of the Rac/Cdc42 effector p21-activated kinase (PAK) and reduced activation of PAK after SCF/SDF1α stimulation (Fig. 1*D*). There were no measurable changes in other kinase signaling pathways, including ERK, JNK, and AKT (Fig. 1*D*). These results suggested that Vav1 may function as a critical signaling molecule regulating HSPC functions.

Abnormal Responses to SDF1α in *Vav1*$^{-/-}$ HSPC. The BM of *Vav1*$^{-/-}$ mice contained normal numbers of immunophenotypically defined long-term HSC, modestly increased frequency of short-term HSC, and slightly reduced numbers of common myeloid progenitors and granulocyte-monocyte progenitors as defined by surface markers (Fig. S1*A*). However, the frequency of functionally defined myeloid progenitors in the BM, as determined by in vitro growth in methylcellulose, was similar to that of WT mice; we did not observe any alterations in the number of colony-forming cells (CFC) obtained in the presence of SCF or granulocyte-colony-stimulating factor (G-CSF) alone or multiple cytokines, or in the frequency of high-proliferation potential colony-forming cells (HPP-CFC), which represent more primitive progenitors (Fig. S1*B*). Moreover, the frequency of cobblestone area-forming cells (CAFC) in *Vav1*$^{-/-}$ BM was virtually identical to that of WT mice both at early (reflecting mature progenitors) and late (representing more primitive HSPC) time points (Fig. S1*C*). Consistent with these data, analysis of the cell cycle (Fig. S1*D*) and apoptosis (Fig. S1*E*) of immunophenotypically defined HSPC subsets in the BM of *Vav1*$^{-/-}$ mice did not reveal any alterations.

We have previously shown that deficiency of the Vav target Rac is associated with massive mobilization of HSPC from the BM. However, analysis of the number of progenitors in peripheral blood of *Vav1*$^{-/-}$ mice unexpectedly revealed significantly decreased numbers of circulating CFC and absence of circadian variation (Fig. 2*A*). Because circadian fluctuations in the numbers of circulating HSPC inversely correlate with periodic changes in SDF1α levels in the BM microenvironment (28), these data suggested an abnormal response of *Vav1*$^{-/-}$ HSPC to SDF1α. To test this hypothesis, we treated *Vav1*$^{-/-}$ and WT mice with the SDF1α receptor (CXCR4) antagonist AMD3100, known to induce HSPC mobilization (29). AMD3100 mobilized only 55% of the number of *Vav1*$^{-/-}$ progenitors that the same treatment induced in WT mice (739 vs. 407 CFC/mL, considering untreated mice as baseline; Fig. 2*B*). G-CSF-induced progenitor mobilization, which is mediated at least in part by SDF1α down-regulation (30) or proteolytic degradation (31) in the BM, was also severely impaired in *Vav1*$^{-/-}$ mice (Fig. 2*C*). Thus, in the absence of Vav1, HSPC are relatively insensitive to physiologic or induced changes in SDF1α levels or activity in the BM in vivo.

SDF1α acts both as a chemoattractant, being the only chemokine known to be active on HSPC (32), and as a signal that increases β_1 integrin affinity for ligand binding in different cell types, including hematopoietic progenitors ("inside-out signaling") (33, 34). To dissect the requirement of Vav1 in SDF1α-mediated HSPC functions, we studied the role of Vav1 in each of

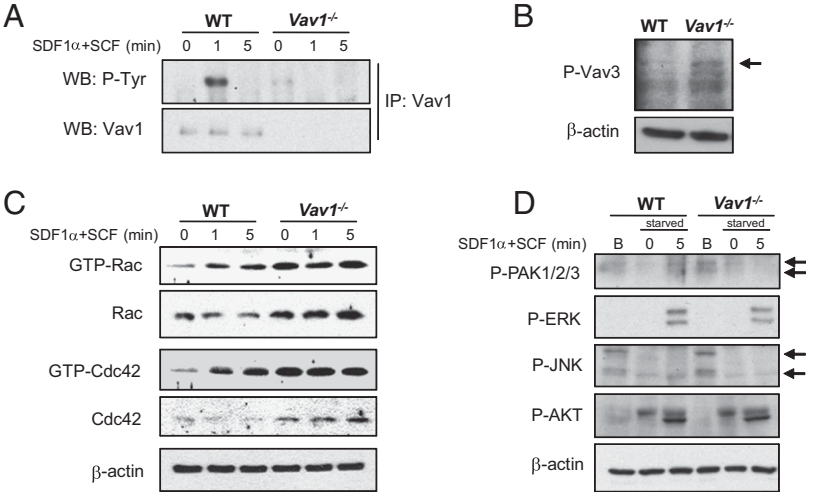

Fig. 1. Dysregulated Rho GTPase activation in *Vav1*$^{-/-}$ hematopoietic progenitors. (*A*) Vav1 activation as demonstrated by immunoprecipitation (IP) with a Vav1-specific antibody, followed by detection with phosphotyrosine (P-Tyr) antibody. WT or *Vav1*$^{-/-}$ lineage-depleted cells were starved in 1% FBS for 6 h and stimulated with SCF + SDF1α (100 ng/mL each) for the indicated time points. WB, Western blot. (*B*) Vav3 phosphorylation in WT and *Vav1*$^{-/-}$ progenitors, detected with a phosphospecific antibody. (*C*) Levels of active (GTP-bound) and total Rac and Cdc42 in WT or *Vav1*$^{-/-}$ lineage-depleted cells. Cells were starved and stimulated as in *A*. GTP-bound Rho GTPases were precipitated with agarose-conjugated PAK1-p21-binding domain (PBD) and detected by Western blot. (*D*) Activation status of different signaling pathways in WT and *Vav1*$^{-/-}$ progenitors, analyzed by Western blot with phosphospecific antibodies. Lineage-depleted cells were either freshly purified (B, baseline activation) or starved in 1% FBS for 6 h and then stimulated with SCF + SDF1α (100 ng/mL each) for the indicated time points. Arrows indicate phospho-Vav3 (*B*) and the different isoforms of phospho-PAK and phospho-JNK (*D*).

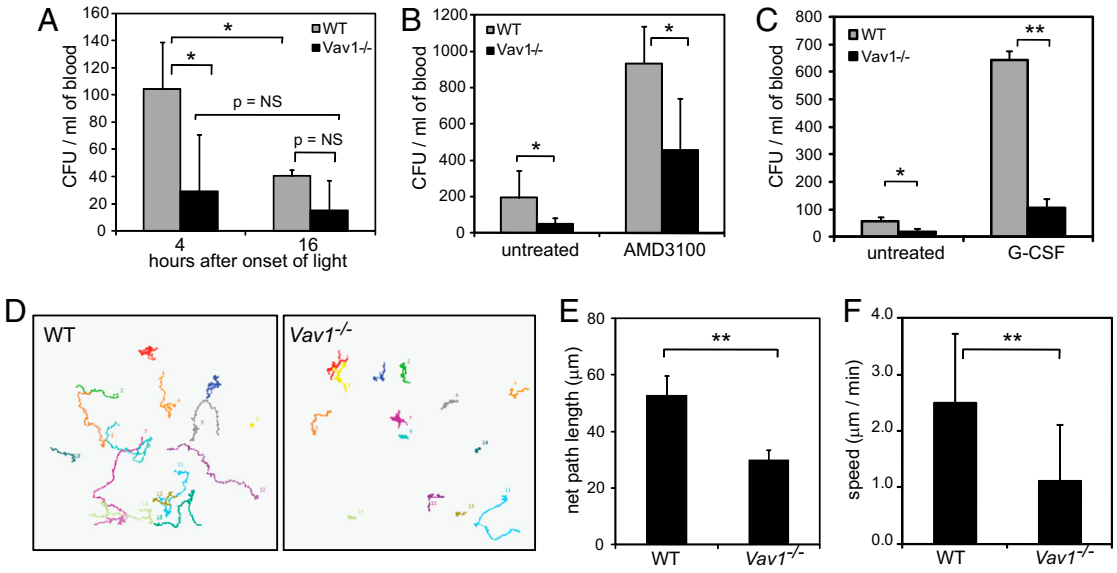

Fig. 2. Abnormal SDF1α responses in *Vav1*$^{-/-}$ HSPC. (*A*) Day–night variation in the number of CFC in peripheral blood of WT and *Vav1*$^{-/-}$ mice. Blood was collected 4 or 16 h after the onset of light. Data represent mean ± SD, $n = 4$–6; *$P < 0.05$ (*t* test). NS, nonsignificant. (*B*) Numbers of CFC in peripheral blood of WT and *Vav1*$^{-/-}$ mice, either untreated or treated with 5 mg/kg of AMD3100 for 1 h. Data represent mean ± SD, $n = 6$–7; *$P < 0.05$ (*t* test). (*C*) Numbers of CFC in peripheral blood of WT and *Vav1*$^{-/-}$ mice, either untreated or treated with G-CSF at a daily dose of 200 μg/kg for 6 d. Data represent mean ± SD, $n = 3$; *$P <$ 0.05, **$P < 0.005$ (*t* test). The graph shows one of two experiments that yielded similar results. (*D*–*F*) In vitro chemotaxis of WT or *Vav1*$^{-/-}$ LSK cells on a fibronectin-coated coverslip in the presence of an SDF1α gradient, determined by time-lapse microscopy. (*D*) Paths followed by individual cells in 1 h. Representative fields (325 × 325 μm) from one out of three similar experiments are shown. (*E*) Net path length migrated in 1 h (mean ± SEM, $n = 36$–38 cells per genotype) and (*F*) speed of migration (mean ± SEM, $n = 14$–41). For *E* and *F*, one representative experiment of a total of three is shown. **$P < 0.005$ (*t* test).

these processes in vitro. *Vav1*$^{-/-}$ lin$^-$ Sca1$^+$ ckit$^+$ (LSK) cells observed by time-lapse microscopy showed significantly abnormal migratory response to an SDF1α gradient (Fig. 2 *D*–*F* and Movies S1 and S2). Compared with WT LSK cells, the distance migrated by *Vav1*$^{-/-}$ cells in 1 h (Fig. 2*E*) and their speed (Fig. 2*F*) were significantly decreased. Absence of Vav1 did not affect the directionality of cell migration. On the other hand, Vav1 was not required for baseline or SDF1α-induced β_1 integrin-mediated adhesion, measured either as static adhesion to fibronectin- or VCAM1-coated plates (Fig. S2*A*) or as the resistance of adherent cells to detachment from an immobilized β_1 integrin ligand under conditions of shear stress (Fig. S2*B*). SDF1α stimulation induced β_1 integrin-mediated firm adhesion of WT and *Vav1*$^{-/-}$ progenitors to a similar extent, suggesting that deletion of Vav1 does not affect SDF1α-mediated inside-out β_1 integrin signaling (Fig. S2*B*). Surface expression of β_1 integrin subunits α_4 and α_5 was similar in WT and *Vav1*$^{-/-}$ LSK or lin$^-$ ckit$^+$ Sca1$^-$ cells (Fig. S2*C*). Together, these data suggest that Vav1 mediates chemotactic but not adhesive responses to SDF1α in HSPC.

Engraftment Defect of *Vav1*$^{-/-}$ HSPC. SDF1α/CXCR4 signaling is required for engraftment and retention of HSPC in the BM after transplantation (8, 9, 35). To further study the role of Vav1 in SDF1α responses in vivo, we determined whether *Vav1*$^{-/-}$ HSPC were able to engraft and reconstitute hematopoiesis. In initial repopulation assays, WT and *Vav1*$^{-/-}$ BM cells were transduced with retroviral vectors encoding two different fluorescent proteins and transplanted into isogenic recipients. In this experimental setting, *Vav1*$^{-/-}$ cells displayed dramatically reduced engraftment ability (Fig. S3). This experiment was also performed with the reverse color combination, with similar results. To eliminate possible effects of in vitro manipulation on engraftment of *Vav1*$^{-/-}$ cells, we performed competitive repopulation assays with freshly isolated, unmanipulated cells. *Vav1*$^{-/-}$ cells did not contribute significantly to donor chimerism in peripheral blood at any time point after transplant (Fig. 3*A*), and were absent from BM and spleen 4 mo posttransplant (Fig. 3*B*). All three lineages examined (myeloid, B-lymphoid, and T-lymphoid) demonstrated defective repopulation in mice transplanted with *Vav1*$^{-/-}$ BM cells (Tables S1 and S2). In contrast, WT BM cells showed stable chimerism at a level consistent with the input (53.5–63.2%), arguing against the possibility that the different genetic background of donor and recipient mice (C57BL/10J versus C57BL/6J) may be responsible for the engraftment failure of *Vav1*$^{-/-}$ cells.

Vav1$^{-/-}$ BM cells also performed poorly in noncompetitive repopulation assays: A fraction of mice (4/10, 40%) transplanted with *Vav1*$^{-/-}$ BM in the absence of competitor cells died within the first month posttransplant, whereas all animals (10/10) receiving WT cells survived (Fig. 3*C*). Surviving mice engrafted with *Vav1*$^{-/-}$ BM showed significantly delayed hematopoietic reconstitution, compared with mice receiving WT cells (Fig. 3*D*). Taken together, these data demonstrate a significant defect in the capacity of *Vav1*$^{-/-}$ HSPC to engraft in transplant reconstitution assays, despite the normal progenitor content and even an elevated frequency of phenotypically defined, short-term HSC in the BM of *Vav1*$^{-/-}$ mice. This phenotype is observed at all time points analyzed, suggesting a defect common to both short- and long-term repopulating cells.

***Vav1*$^{-/-}$ HSPC Show Abnormal Homing Toward Nestin$^+$ MSC.** To gain further mechanistic insight into this engraftment defect, we studied the role of Vav1 in HSPC homing and microlocalization in the BM. *Vav1*$^{-/-}$ HSPC showed normal homing efficiency as determined by CFC assay at 16 h (Fig. 4*A*) and by intravital microscopy of 1,1′-dioctadecyl-3,3,3′,3′-tetramethylindodicarbocyanine perchlorate (DiD)-labeled LSK cells 1 h posttransplant (Fig. 4*B*). Therefore, Vav1 is not required for initial homing of HSPC into the BM cavity. Because SDF1α is expressed at highest levels by perivascular nestin$^+$ MSC (6) and at lower levels by other cell populations including osteoblasts (5, 36, 37), we directly visualized the homing of DiD-labeled WT or *Vav1*$^{-/-}$ LSK cells to defined regions of the calvarium BM using intravital microscopy (7). The use of two transgenic reporter mouse strains, Nestin-GFP and Col2.3-GFP, allowed the study of HSPC localization with respect to perivascular nestin$^+$ MSC and osteoblastic cells, respectively.

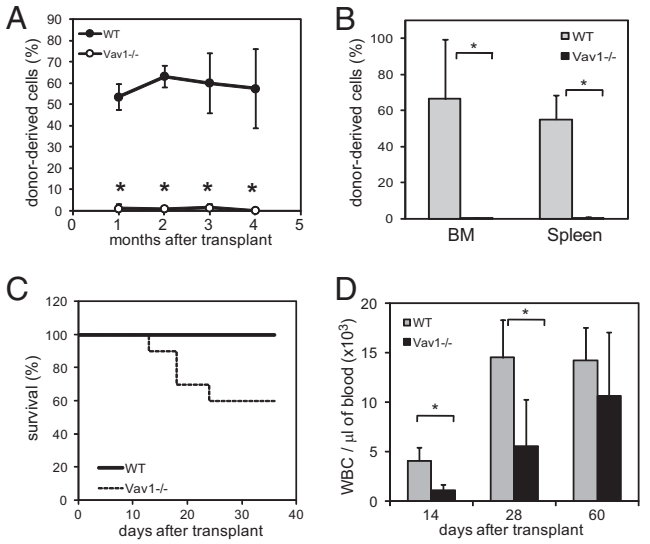

Fig. 3. Engraftment defect of *Vav1*$^{-/-}$ BM cells. (*A*) Peripheral blood chimerism of lethally irradiated B6.SJL (CD45.1) mice transplanted with 3×10^6 WT or *Vav1*$^{-/-}$ (CD45.2) BM cells and an equal number of WT CD45.1 BM cells as competitors. (*B*) CD45.2 chimerism in BM and spleen for the recipient mice in *A*, killed 4 mo posttransplant. Data in *A* and *B* are expressed as the percentage of CD45.2$^+$ cells in the nucleated fractions measured by flow cytometry. Mean ± SD, $n = 5$, $^*P < 0.005$ (*t* test). Note: Chimerism for *Vav1*$^{-/-}$ cells in BM and spleen was less than 2%. (*C*) Survival of lethally irradiated B6.SJL mice transplanted with 3×10^6 WT or *Vav1*$^{-/-}$ (CD45.2) BM cells in the absence of competitor cells; $n = 10$ mice per genotype. (*D*) Leukocyte counts in peripheral blood of the recipient mice in *C* surviving at each time point. Mean ± SD, $n = 6$–10, $^*P < 0.005$ (*t* test).

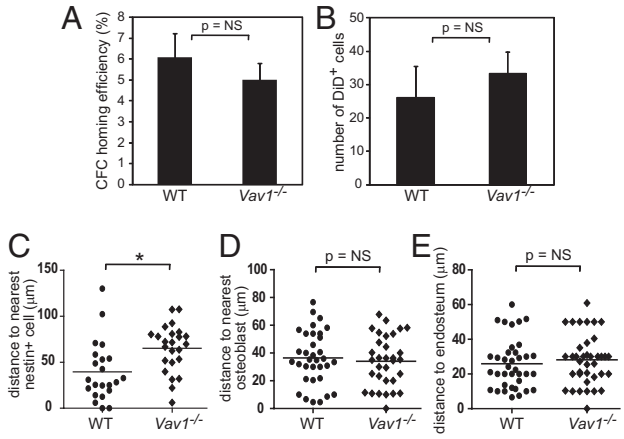

Fig. 4. Bone marrow homing and localization of *Vav1*$^{-/-}$ HSPC. (*A*) Homing efficiency of WT and *Vav1*$^{-/-}$ progenitors (CFC) to the BM of C57BL/10J recipients 16 h after transplant. Data represent mean ± SD, $n = 5$. (*B*) Number of DiD$^+$ LSK cells detected by intravital microscopy in a 4×6 mm region of the calvarium of Col2.3-GFP mice 1 h after transplant, for an input of 30,000 LSK cells (mean ± SD, $n = 3$). (*C*–*E*) Distances (in µm) of transplanted LSK cells to nestin$^+$ cells (*C*), osteoblastic cells (*D*), and endosteal surface (*E*) in the calvarium of Nestin-GFP (*C*) or Col2.3-GFP (*D* and *E*) mice, determined 1 h after transplant. Data represent measurements for individual LSK cells; horizontal lines represent the mean. *C* represents pooled data from three mice per genotype ($n = 24$–32); *D* and *E* represent data from one representative mouse per genotype, out of three analyzed ($n = 32$–34; total number of events analyzed, $n = 77$–98). $^*P = 0.005$ (*t* test).

Compared with WT HSPC, *Vav1*$^{-/-}$ HSPC localized significantly farther from nestin$^+$ cells 1 h after transplant. Only 6.25% of *Vav1*$^{-/-}$ HSPC, compared with 45.8% of WT HSPC, were located less than 30 µm from a nestin$^+$ cell ($n = 24$–32 HSPC analyzed). In addition, 25% of *Vav1*$^{-/-}$ HSPC versus only 8.3% of WT HSPC were found in microscopic fields (330 × 330 µm) lacking nestin$^+$ cells. Considering only WT and *Vav1*$^{-/-}$ HSPC with nestin$^+$ cells in their proximity, the mean distance of HSPC to the nearest nestin$^+$ cell was significantly shorter for WT versus *Vav1*$^{-/-}$ HSPC (WT, 39.54 ± 6.91 µm; *Vav1*$^{-/-}$, 65.24 ± 5.22 µm; $n = 22$–24; $P = 0.005$) (Fig. 4*C* and Fig. S4). In contrast, the distribution of *Vav1*$^{-/-}$ HSPC relative to osteoblasts (Fig. 4*D* and Fig. S4) and endosteal surface (Fig. 4*E*) 1 h after transplant was not significantly different from that of WT HSPC ($n = 77$–98 HSPC analyzed).

Impaired Retention of *Vav1*$^{-/-}$ HSPC in the BM Niche. To assess retention of transplanted HSPC in the BM, we examined by intravital microscopy the number and localization of DiD-labeled LSK cells present in the calvarium BM cavity at 48 h posttransplant. Contrary to the earlier time point, the total number of *Vav1*$^{-/-}$ LSK cells in the BM cavity at 48 h was significantly decreased, compared with WT cells in both Nestin-GFP and Col2.3-GFP recipients (60% and 44% reduction, respectively; $P < 0.05$ for both strains, for a total of three to five recipient mice analyzed per strain and genotype; Fig. 5*A*), suggesting impaired retention. At this time point, there was not any significant difference in the localization of retained *Vav1*$^{-/-}$ HSPC with respect to nestin$^+$ cells, osteoblasts, or endosteal surface, compared with WT HSPC (Fig. 5 *B*–*D*). We attempted to determine whether this reduction in the number of donor cells in the BM correlated with their increase in circulation; however, the numbers of circulating donor cells detected at this time point (<0.25% donor chimerism in peripheral blood 48 h after transplant of 1.5×10^5 lin$^-$ ckit$^+$ cells, for both genotypes) was too low to allow any conclusions.

Although *Vav1*$^{-/-}$ HSPC did not demonstrate any alteration in proliferation or apoptosis (Fig. S1*D* and *E*) in primary mice during homeostatic hematopoiesis, it was still possible that defects in the proliferation or survival of these cells following transplantation—rather than reduced retention—could account for the reduced numbers of *Vav1*$^{-/-}$ HSPC observed at the 48 h imaging time point. To determine the proliferation status of transplanted hematopoietic progenitors shortly after the initial BM homing, we injected WT or *Vav1*$^{-/-}$ lin$^-$ ckit$^+$ cells into lethally irradiated recipients, which were pulsed with BrdU 48 h after transplant. There was no significant difference in the fraction of donor-derived (CD45.2$^+$) BM cells incorporating BrdU between the two genotypes (45.8 ± 6.10% vs. 50.5 ± 5.8%, WT vs. *Vav1*$^{-/-}$, $n = 5$–6 mice per genotype; Fig. S5*A*). An independent measure of HSPC proliferation after transplant was obtained from in vivo imaging experiments, in which the presence of clusters of DiD$^+$ cells with a reduction in dye intensity can be taken as an indication of proliferation of single transplanted cells (7). The fraction of proliferating LSK cells, as determined by the percentage of cell clusters 48 h after transplant, was similar for WT and *Vav1*$^{-/-}$ cells (38.0 ± 12.4% vs. 42.9 ± 14.2%, WT vs. *Vav1*$^{-/-}$, $n = 4$–5 mice per genotype; Fig. S5*B*), consistent with the BrdU-labeling studies. Likewise, the fraction of lin$^-$ ckit$^+$ cells that were apoptotic (Annexin V$^+$) 48 h after transplant was not significantly different between the two genotypes (Fig. S5*C*). These data are consistent with normal ERK, JNK, and AKT activation previously noted (Fig. 1*B*) and support the hypothesis that the failure of *Vav1*$^{-/-}$ cells to engraft is due to reduced retention in the BM. Taken together, these data imply that Vav1 is required in HSPC for a normal response to SDF1α leading to Rac/Cdc42 activation, perivascular localization, retention in the BM niche, and engraftment.

Discussion

Previous work has demonstrated that Rho GTPases function as central molecules critical for the interaction of HSPC with the BM hematopoietic microenvironment. Inactivation of Rac1 alone

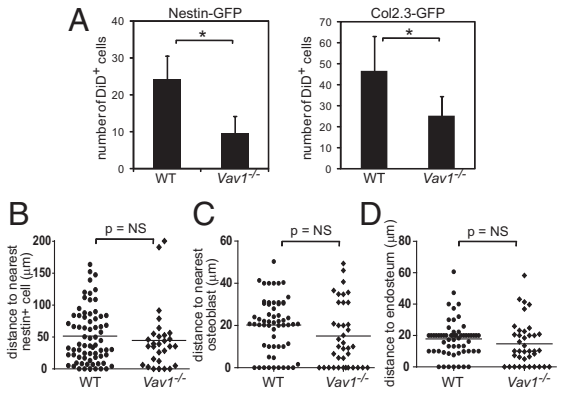

Fig. 5. Reduced retention of *Vav1*$^{-/-}$ HSPC in the BM. (*A*) Number of DiD$^+$ LSK cells detected by intravital microscopy in a 4 × 6 mm region of the calvarium of Nestin-GFP and Col2.3-GFP mice 48 h after transplant (mean ± SD, n = 4–5) for an input of 30,000 LSK cells. *$P < 0.05$ (t test). (*B–D*) Distances (in μm) of transplanted LSK cells to nestin$^+$ cells (*B*), osteoblastic cells (*C*), and endosteal surface (*D*) in the calvarium of Nestin-GFP (*B*) or Col2.3-GFP (*C* and *D*) mice, determined 48 h after transplant. Data represent measurements for individual LSK cells; horizontal lines represent the mean. *B* represents pooled data from three mice per genotype (n = 29–71); *C* and *D* represent data from one representative mouse per genotype, out of three analyzed (n = 38–59; total number of events analyzed, n = 102–139).

impairs HSPC engraftment, whereas deletion of both Rac1 and Rac2 (13, 14) or Cdc42 (15) leads to massive egress of HSPC from the BM. Rac and Cdc42 are activated by multiple receptors via a large family of Rho GEFs, of which ∼70 members have been described so far (17). Thus, genetic studies examining the phenotype of Rho GTPase knockouts, even when performed in a lineage-specific fashion, likely demonstrate the combinatorial effects of multiple receptors and downstream signaling pathways. Indeed, one of the challenges in understanding the specific roles of chemokine and adhesion receptors in HSPC function is that many downstream GEFs may activate multiple Rho GTPases in an apparently redundant and cell- or agonist-specific fashion.

Here we have demonstrated a role for Vav1 as a key functional regulator of Rac/Cdc42 in HSPC, as shown by the fact that deletion of this single GEF completely alters Rho GTPase activation patterns in hematopoietic progenitors. *Vav1*$^{-/-}$ progenitors show defective activation of Rac and Cdc42 and their effector PAK in response to SDF1α and SCF, agonists previously shown to activate Rac in HSPC and critical in HSPC engraftment. Unexpectedly, however, *Vav1*$^{-/-}$ progenitors also showed baseline hyperactivation of Rac and Cdc42, probably due to compensatory hyperactivation of Vav2/Vav3.

Although Vav- and Rac-deficient HSPC exhibit similar engraftment defects in repopulation assays, their phenotypes are in most other respects remarkably different, allowing a more precise dissection of the critical pathways regulating HSPC trafficking and interaction with the hematopoietic microenvironment. Whereas Rac-deficient HSPC show alterations in multiple cellular processes involved in engraftment and retention (SCF-induced proliferation, chemotaxis, homing, survival, and β_1 integrin-mediated adhesion), the engraftment failure of *Vav1*$^{-/-}$ HSPC appears to be specifically associated with a much more restricted defect: abnormal response to SDF1α leading to abnormal localization and reduced retention, underscoring the key role of this distinct pathway in HSPC engraftment. Interestingly, the lack of postengraftment retention is not related to the absence of any immunophenotypically or in vitro defined HSPC population in *Vav1*$^{-/-}$ mice, suggesting that signaling pathways are qualitatively or quantitatively differentially used in posttransplant versus ontogenic migration and expansion of HSPC. On the other hand, *Vav1*$^{-/-}$ and *Rac1*$^{-/-}$*;Rac2*$^{-/-}$ mice unexpectedly show opposite mobilization phenotypes, with decreased versus highly increased numbers of circulating progenitors, respectively. The findings that both *Vav1*$^{-/-}$ and *Rac1*$^{-/-}$ HSPC, which have normal β_1 integrin-mediated adhesion, do not show increased mobilization, whereas *Rac2*$^{-/-}$ and *Rac1*$^{-/-}$*;Rac2*$^{-/-}$ HSPC mobilize in inverse correlation to their decreased binding to fibronectin, imply that HSPC mobilization may be more dependent on loss of integrin-mediated adhesion than on migration per se, at least as measured by in vitro assays.

These data also suggest that different Rho GEFs play selective roles downstream of different extracellular signals, thus controlling distinct cellular processes. Thus, inactivation of other GEFs expressed in HSPC leads to phenotypes strikingly different from *Vav1*$^{-/-}$. Similar to combined genetic deletion of Rac1 and Rac2, pharmacologic inhibition of Tiam1/Trio-mediated Rac activation by NSC23766 induces HSPC mobilization (13), suggesting that these GEFs may be required for integrin-mediated Rac activation and HSPC adhesion. Conversely, deletion of Vav1, which is not targeted by NSC23766 (38), does not affect adhesion nor induce mobilization but leads to defective SDF1α responses.

Vav1 is required for appropriate HSPC responses to SDF1α under both physiologic conditions and in the posttransplant hematopoietic microenvironment. Thus, *Vav1*$^{-/-}$ HSPC showed impaired in vitro chemotaxis; reduced mobilization induced by AMD3100 or G-CSF (both of which depend on CXCR4/SDF1α inactivation); absence of physiologic, circadian mobilization [related to oscillations in SDF1α levels in the BM (28)]; and reduced homing to the proximity of SDF1α-expressing nestin$^+$ MSC, recently implicated as perivascular cells that contribute to the HSC niche and are required for HSC maintenance (6). These observations delineate a specific requirement for Vav1 in the proposed role of the CXCR4/SDF1α axis in the regulation of HSPC trafficking and engraftment. Although initial data showed that homing of HSPC is blocked by anti-CXCR4 antibodies (39), subsequent studies found that *Cxcr4*$^{-/-}$ progenitors home normally (8), which is consistent with our findings in *Vav1*$^{-/-}$ cells. Taken together, these studies suggest that this pathway is dispensable for the initial BM homing. However, CXCR4 signaling is required for the engraftment and retention of human HSPC in non-obese diabetic (NOD)/SCID mice (9), and murine *Cxcr4*$^{-/-}$ HSPC show reduced retention in the BM microenvironment after transplantation (8, 35), which parallels our observations with *Vav1*$^{-/-}$ HSPC. Together, these data support the idea that the initial bone marrow homing and subsequent retention are two components of the engraftment process with distinct biochemical regulation.

Vav1$^{-/-}$ HSPC appear to retain partial responsiveness to an SDF1α gradient, being able to migrate short distances and being mobilized at lower levels by AMD3100. Vav2 and Vav3, which have been shown to play both unique and overlapping roles in lymphocytes, may play partially compensatory roles in some of the migratory and adhesive functions of HSPC, which may allow the retention of *Vav1*$^{-/-}$ HSPC under steady-state conditions but may not be sufficient under the more stringent conditions of a BM transplant. Vav3 (and possibly Vav2) is hyperactivated in unstimulated *Vav1*$^{-/-}$ progenitors (Fig. 1*B*).

The defect in early localization of *Vav1*$^{-/-}$ HSPC near nestin$^+$ MSC correlates with impaired BM retention and engraftment. In contrast, correct positioning of *Vav1*$^{-/-}$ HSPC with respect to osteoblastic cells or the matrix of the endosteal surface was not sufficient for functional engraftment. These data do not rule out a role for the osteoblastic space in long-term HSPC maintenance; however, they support the idea that localization in the proximity of a perivascular mesenchymal cell is required in the initial stages of HSPC homing and is important for their early retention. Nestin$^+$ MSC are major producers of SDF1α in the BM (6), and we have shown that Vav1 is required for appropriate responses of HSPC to SDF1α, consistent with the abnormal localization of *Vav1*$^{-/-}$ HSPC in the perivascular, SDF1α-abundant space. Thus, we describe a signaling pathway differentially reg-

ulating HSPC localization with respect to perivascular versus osteoblastic niche components.

Together, our data imply that the hematopoietic-specific GEF Vav1 is essential for the correct response of HSPC to SDF1α in the BM microenvironment, leading to Rac/Cdc42 activation, perivascular localization, retention in the BM niche, and subsequent engraftment, and define a critical biochemical pathway in the regulation of Rho GTPase activity in HSPC.

Methods

Mice. All procedures involving mice followed Children's Hospital Boston Institutional Animal Care and Use Committee guidelines. *Vav1*$^{-/-}$ mice have been previously reported (20) and were backcrossed into a C57BL/10J (CD45.2) background. Age- (8- to 16-wk-old) and sex-matched C57BL/10J mice (Jackson Laboratory) were used as WT controls. B6.SJL (CD45.1) mice (Jackson Laboratory) were used as recipients in some transplant assays. All recipient mice were lethally irradiated (^{137}Cs source, 11.5-Gy whole-body irradiation) before BM transplant.

Transplants, Progenitor Assays, and Flow Cytometry. Hematopoietic repopulation ability was assessed in both competitive and noncompetitive assays (see *SI Methods* for details). Progenitor content in BM and peripheral blood was determined by methylcellulose CFC assays, as previously described (13, 14). The frequency of circulating HSPC was determined under different conditions (diurnal vs. nocturnal, AMD3100, G-CSF). In vivo HSPC proliferation and apoptosis were determined by BrdU incorporation and Annexin V binding assays (BD Biosciences), respectively, either in primary, unmanipulated mice or in transplanted lin$^-$ ckit$^+$ cells 48 h posttransplant. Biochemical assays, immunophenotyping, and progenitor homing assays were performed essentially as described elsewhere (13, 14).

Chemotaxis and Adhesion Assays. In vitro migration in response to SDF1α was measured by time-lapse microscopy in Dunn chemotaxis chambers, as described (14) (see also *SI Methods*). Static adhesion assays were performed as previously described (13, 14). Firm adhesion and the effect of SDF1α on adhesion were measured with a computer-operated flow-chamber device (Mirus Nanopump; Cellix; *SI Methods*).

Intravital Microscopy. HSPC microlocalization in the BM was analyzed by intravital microscopy using previously described equipment and procedures (7). The use of two transgenic reporter mouse strains, nestin-GFP and Col2.3-GFP, allowed the study of HSPC localization with respect to perivascular nestin$^+$ MSC and osteoblastic cells, respectively. Cells were imaged at two time points posttransplant, 1 h (to determine the initial homing and localization) and 48 h (to assess short-term retention and the effect of proliferation as determined by clusters of DiD$^+$ cells with generally reduced dye intensity).

ACKNOWLEDGMENTS. We thank Stuart Orkin, Leonard Zon, Jose Cancelas, and members of our laboratories for discussing and critically reading the manuscript. Charles P. Lin and Joel Spencer assisted with intravital microscopy, Ronald Mathieu assisted with cell sorting, Chad Harris and Megan Bariteau provided technical support, and Elise Porter provided administrative assistance. This work was supported by National Institutes of Health Grants DK62757 (to D.A.W.) and HL44851, HL097794, and HL081030 (to D.T.S.).

1. Wilson A, Trumpp A (2006) Bone-marrow haematopoietic-stem-cell niches. *Nat Rev Immunol* 6:93–106.
2. Calvi LM, et al. (2003) Osteoblastic cells regulate the haematopoietic stem cell niche. *Nature* 425:841–846.
3. Zhang J, et al. (2003) Identification of the haematopoietic stem cell niche and control of the niche size. *Nature* 425:836–841.
4. Kiel MJ, et al. (2005) SLAM family receptors distinguish hematopoietic stem and progenitor cells and reveal endothelial niches for stem cells. *Cell* 121:1109–1121.
5. Sugiyama T, Kohara H, Noda M, Nagasawa T (2006) Maintenance of the hematopoietic stem cell pool by CXCL12-CXCR4 chemokine signaling in bone marrow stromal cell niches. *Immunity* 25:977–988.
6. Méndez-Ferrer S, et al. (2010) Mesenchymal and haematopoietic stem cells form a unique bone marrow niche. *Nature* 466:829–834.
7. Lo Celso C, et al. (2009) Live-animal tracking of individual haematopoietic stem/progenitor cells in their niche. *Nature* 457:92–96.
8. Foudi A, et al. (2006) Reduced retention of radioprotective hematopoietic cells within the bone marrow microenvironment in CXCR4$^{-/-}$ chimeric mice. *Blood* 107: 2243–2251.
9. Peled A, et al. (1999) Dependence of human stem cell engraftment and repopulation of NOD/SCID mice on CXCR4. *Science* 283:845–848.
10. Papayannopoulou T, Craddock C, Nakamoto B, Priestley GV, Wolf NS (1995) The VLA4/VCAM-1 adhesion pathway defines contrasting mechanisms of lodgement of transplanted murine hemopoietic progenitors between bone marrow and spleen. *Proc Natl Acad Sci USA* 92:9647–9651.
11. Scott LM, Priestley GV, Papayannopoulou T (2003) Deletion of α4 integrins from adult hematopoietic cells reveals roles in homeostasis, regeneration, and homing. *Mol Cell Biol* 23:9349–9360.
12. Williams DA, Rios M, Stephens C, Patel VP (1991) Fibronectin and VLA-4 in haematopoietic stem cell-microenvironment interactions. *Nature* 352:438–441.
13. Cancelas JA, et al. (2005) Rac GTPases differentially integrate signals regulating hematopoietic stem cell localization. *Nat Med* 11:886–891.
14. Gu Y, et al. (2003) Hematopoietic cell regulation by Rac1 and Rac2 guanosine triphosphatases. *Science* 302:445–449.
15. Yang L, et al. (2007) Rho GTPase Cdc42 coordinates hematopoietic stem cell quiescence and niche interaction in the bone marrow. *Proc Natl Acad Sci USA* 104: 5091–5096.
16. Williams DA, Zheng Y, Cancelas JA (2008) Rho GTPases and regulation of hematopoietic stem cell localization. *Methods Enzymol* 439:365–393.
17. Rossman KL, Der CJ, Sondek J (2005) GEF means go: Turning on RHO GTPases with guanine nucleotide-exchange factors. *Nat Rev Mol Cell Biol* 6:167–180.
18. Turner M, Billadeau DD (2002) VAV proteins as signal integrators for multi-subunit immune-recognition receptors. *Nat Rev Immunol* 2:476–486.
19. Tarakhovsky A, et al. (1995) Defective antigen receptor-mediated proliferation of B and T cells in the absence of Vav. *Nature* 374:467–470.
20. Turner M, et al. (1997) A requirement for the Rho-family GTP exchange factor Vav in positive and negative selection of thymocytes. *Immunity* 7:451–460.
21. Zhang R, Alt FW, Davidson L, Orkin SH, Swat W (1995) Defective signalling through the T- and B-cell antigen receptors in lymphoid cells lacking the vav proto-oncogene. *Nature* 374:470–473.
22. Fujikawa K, et al. (2003) Vav1/2/3-null mice define an essential role for Vav family proteins in lymphocyte development and activation but a differential requirement in MAPK signaling in T and B cells. *J Exp Med* 198:1595–1608.
23. Gakidis MA, et al. (2004) Vav GEFs are required for β2 integrin-dependent functions of neutrophils. *J Cell Biol* 166:273–282.
24. Graham DB, et al. (2007) Neutrophil-mediated oxidative burst and host defense are controlled by a Vav-PLCγ2 signaling axis in mice. *J Clin Invest* 117:3445–3452.
25. Phillipson M, et al. (2009) Vav1 is essential for mechanotactic crawling and migration of neutrophils out of the inflamed microvasculature. *J Immunol* 182:6870–6878.
26. Carstanjen D, et al. (2005) Rac2 regulates neutrophil chemotaxis, superoxide production, and myeloid colony formation through multiple distinct effector pathways. *J Immunol* 174:4613–4620.
27. Yang FC, et al. (2000) Rac2 stimulates Akt activation affecting BAD/Bcl-XL expression while mediating survival and actin function in primary mast cells. *Immunity* 12: 557–568.
28. Méndez-Ferrer S, Lucas D, Battista M, Frenette PS (2008) Haematopoietic stem cell release is regulated by circadian oscillations. *Nature* 452:442–447.
29. Broxmeyer HE, et al. (2005) Rapid mobilization of murine and human hematopoietic stem and progenitor cells with AMD3100, a CXCR4 antagonist. *J Exp Med* 201: 1307–1318.
30. Semerad CL, et al. (2005) G-CSF potently inhibits osteoblast activity and CXCL12 mRNA expression in the bone marrow. *Blood* 106:3020–3027.
31. Petit I, et al. (2002) G-CSF induces stem cell mobilization by decreasing bone marrow SDF-1 and up-regulating CXCR4. *Nat Immunol* 3:687–694.
32. Wright DE, Bowman EP, Wagers AJ, Butcher EC, Weissman IL (2002) Hematopoietic stem cells are uniquely selective in their migratory response to chemokines. *J Exp Med* 195:1145–1154.
33. Hidalgo A, et al. (2001) Chemokine stromal cell-derived factor-1α modulates VLA-4 integrin-dependent adhesion to fibronectin and VCAM-1 on bone marrow hematopoietic progenitor cells. *Exp Hematol* 29:345–355.
34. Peled A, et al. (2000) The chemokine SDF-1 activates the integrins LFA-1, VLA-4, and VLA-5 on immature human CD34(+) cells: Role in transendothelial/stromal migration and engraftment of NOD/SCID mice. *Blood* 95:3289–3296.
35. Ma Q, Jones D, Springer TA (1999) The chemokine receptor CXCR4 is required for the retention of B lineage and granulocytic precursors within the bone marrow microenvironment. *Immunity* 10:463–471.
36. Jung Y, et al. (2006) Regulation of SDF-1 (CXCL12) production by osteoblasts; a possible mechanism for stem cell homing. *Bone* 38:497–508.
37. Sipkins DA, et al. (2005) In vivo imaging of specialized bone marrow endothelial microdomains for tumour engraftment. *Nature* 435:969–973.
38. Gao Y, Dickerson JB, Guo F, Zheng J, Zheng Y (2004) Rational design and characterization of a Rac GTPase-specific small molecule inhibitor. *Proc Natl Acad Sci USA* 101:7618–7623.
39. Kollet O, et al. (2001) Rapid and efficient homing of human CD34(+)CD38(–/low) CXCR4(+) stem and progenitor cells to the bone marrow and spleen of NOD/SCID and NOD/SCID/B2m(null) mice. *Blood* 97:3283–3291.

Supporting Information

Sanchez-Aguilera et al. 10.1073/pnas.1102018108

SI Methods

Mice. All protocols were approved by the Children's Hospital Boston Institutional Animal Care and Use Committee. Age- and sex-matched *Vav1*$^{-/-}$ (1) and wild-type (WT) C57BL/10J mice (Jackson Laboratory) were used between 8 and 16 wk of age. B6.SJL (CD45.1) mice (Jackson Laboratory) were used as recipients in competitive transplant assays. B6.SJL and C57BL/10J carry identical major histocompatibility complex haplotypes (http://www.jax.org/phenome), and WT C57BL/10J BM cells stably engraft B6.SJL recipients (Fig. 3). All recipients were lethally irradiated (^{137}Cs source, 11.5-Gy whole-body irradiation, split dose 7.5 + 4.0 Gy, 3 h apart) before bone marrow (BM) transplant.

Biochemical Assays. Rac/Cdc42 activation assays were performed on lineage-depleted cells (either freshly isolated or starved for 6 h in Iscove's modified Dulbecco's medium (IMDM), 1% FBS, and then stimulated as required) as previously described (2).

For the detection of Vav1 phosphorylation, 1×10^6 lin$^-$ cells were lysed in 20 mM Tris HCl (pH 8), 150 mM NaCl, 10% glycerol, 1% Triton X-100, 2 mM EDTA, 10 mM NaF, 1 mM Na_3VO_4, and Complete protease inhibitors (Roche). Lysates were incubated with 2 μg of Vav1 antibody (B_6; Santa Cruz Biotechnology) overnight at 4 °C. After addition of 40 μL of protein A/G-agarose (Santa Cruz Biotechnology), lysates were incubated for another 4 h at 4 °C. The beads were washed five times in lysis buffer and boiled in 2× Laemmli sample buffer, and the bound fractions were analyzed by immunoblot.

For immunoblot, the following primary antibodies were used at a 1:1,000 dilution except where otherwise indicated: Rac (clone 102) and Cdc42 (clone 44), from BD Biosciences; Vav1 (2502), phospho-PAK1/2/3 (Ser199/204), phospho-p44/p42 MAPK (Thr202/Tyr204; 197G2), phospho-JNK (Thr183/Tyr185), phospho-p38 (Thr180/Tyr182; 28B10), phospho-AKT (Ser473), from Cell Signaling Technology; phosphotyrosine (4G10) from Millipore; phospho-Vav3, from BioSource; and β-actin (AC-15; 1:10,000 dilution) from Sigma.

Flow Cytometry. Bones (femora, tibiae, and iliac crests) were crushed in a mortar, and single-cell suspensions were prepared from WT and *Vav1*$^{-/-}$ mice. Red blood cells were lysed by incubation in BD PharmLyse (BD Biosciences) for 10 min. Cells ($1–2 \times 10^6$ cells per sample) were incubated with a 1:100 dilution (2–5 μg/mL) of fluorescent antibody conjugates and 4′,6-diamidino-2-phenylindole (DAPI) (0.2 μg/mL; Sigma) for dead cell exclusion, and analyzed on an LSR II flow cytometer (BD Biosciences). The following antibody conjugates were used: CD45.1-FITC (A20), CD45.2-phycoerythrin (PE) (104), c-kit-APC (2B8), Flk2-PE (A2F10.1), CD49d-FITC (R1-2), CD49e-PE (5H10-27), and biotinylated or PE-conjugated CD11b (M1/70), Gr-1 (RB6-8C5), Ter119, B220 (RA3-6B2), CD3ε (145-2C11), CD4 (GK1.5), and CD8a (53-6.7), from BD Biosciences; and FITC- or PE-Cy5.5-conjugated Sca-1 (D7), CD34-FITC (RAM34), CD16/32-Pacific blue (93), IL7Rα-PE-Cy7 (A7R34), from eBioscience. Biotinylated antibodies were detected with streptavidin-APC-Cy7 (BD Biosciences). Phenotypic populations of hematopoietic stem and progenitor cells (HSPC) were defined according to the following scheme: long-term hematopoietic stem cells (HSC) [lin$^-$ Sca1$^+$ ckit$^+$ (LSK) CD34$^-$ Flk2$^-$], short-term HSC (LSK CD34$^+$ Flk2$^-$), multipotential progenitors (MPP) (LSK CD34$^+$ Flk2$^+$), common myeloid progenitors (CMP) (lin$^-$ Sca1$^-$ ckit$^+$ CD34$^+$ FcγRIII/II$^-$), granulocytic-monocytic progenitors (GMP) (lin$^-$ Sca1$^-$ ckit$^+$ CD34$^+$ FcγRIII/II$^+$), and megakaryocytic-erythroid progenitors (MEP) (lin$^-$ Sca1$^-$ ckit$^+$ CD34$^-$ FcγRIII/II$^-$).

Cell-Cycle and Apoptosis Analysis in Vivo. For the determination of cell-cycle status in immunophenotypically defined HSPC, mice were injected intraperitoneally with 1 mg of 5-bromo-2′-deoxyuridine (BrdU) (BD Biosciences) and killed 4 h later. BM cells were first incubated with surface antibodies (lin, ckit, Sca1, CD34, Flk2), then fixed, permeabilized, and stained using the APC BrdU Flow Kit (BD Biosciences), following the manufacturer's instructions. To determine apoptosis levels, BM cells were first stained with surface antibodies and then with Annexin V-APC (BD Biosciences) and DAPI (0.2 μg/mL).

For the analysis of proliferation and apoptosis of transplanted HSPC, 1.5×10^5 WT or *Vav1*$^{-/-}$ lin$^-$ ckit$^+$ cells were injected into B6.SJL recipients. Mice were treated with 1 mg BrdU 48 h post-transplant and killed 12 h later. Red cell-lysed BM cells were incubated with CD45.1-FITC and CD45.2-PE antibodies, and then either fixed and stained with anti-BrdU to determine their cell-cycle status or stained with Annexin V-APC and 7-aminoactinomycin D to measure apoptosis levels.

Colony-Forming Cell and Cobblestone Area-Forming Cell Assays. Methylcellulose colony-forming cell (CFC) assays and high-proliferation potential (HPP)-CFC were performed as previously described (2). Limiting-dilution cobblestone area-forming cell (CAFC) assays were performed on FBMD-1 stromal cells as described elsewhere (2, 3) and the frequency of CAFC was calculated by Poisson statistics using L-Calc software (StemCell Technologies).

Mobilization Assays. Untreated mice were bled at 4 and 16 h after the onset of light to determine circadian variations in circulating CFC. HSPC mobilization was induced with AMD3100 octahydrochloride hydrate (Sigma) (5 mg/kg for 1 h, s.c.) or rhG-CSF (Amgen) (daily dose of 200 μg/kg for 6 d, i.p.). CBC counts were obtained using a Hemavet 950 analyzer (Drew Scientific). After red cell lysis, peripheral blood cells were plated in methylcellulose for determination of progenitor content as described above.

In Vitro Chemotaxis Assays. In vitro chemotaxis in response to stromal derived factor-1 alpha (SDF1α) was analyzed by time-lapse microscopy as previously described (4). Approximately 50,000 LSK cells were plated for 1 h on a fibronectin-coated glass coverslip, which was then placed in a Dunn chemotaxis chamber (Hawksley). SDF1α (100 ng/mL) was added as a chemoattractant in the outer well, and cells were imaged for 1 h at 30-s intervals using an Eclipse Ti microscope and NIS-Elements software (Nikon). Cell tracking and calculations of distance, speed, and directionality were performed with DIAS 3.0 software (Soll Technologies).

In Vitro Adhesion Assays. To determine static adhesion of hematopoietic progenitors to different substrates in vitro, low-density bone marrow cells (300,000 cells per well) in complete medium were plated in triplicate on 24-well non-tissue culture-treated plates previously coated with fibronectin (CH-296, 30 μg/mL; Takara Bio) or VCAM1-Fc (20 μg/mL; R&D Systems). Cells were incubated for 1 h at 37 °C, after which the supernatant was removed and the wells were washed once with PBS to remove nonadherent cells. Adherent cells were harvested by treatment with Cell Dissociation Buffer, enzyme-free (Invitrogen) and plated in methylcellulose. Progenitor adhesion was determined as the

percentage of CFC in the adherent fractions, relative to the frequency of CFC in the input sample.

Resistance of integrin-mediated adhesion to shear stress was measured using Vena8 biochips connected to a Mirus Nanopump syringe pump (Cellix). Biochips were coated with VCAM1-Fc (1 μg/mL) and SDF1α (10 μg/mL), or with VCAM1-Fc alone. Lin^- $ckit^+$ cells (100,000 per well) were injected into one of the microcapillaries of the biochip, allowed to adhere statically for 5 min at 37 °C, and then subjected to increasing shear stress rates (1–15 dyne/cm^2) in 1-min segments. The biochip was imaged by time-lapse microscopy, and the number of adherent cells at the end of each flow rate segment was determined using ImageJ software (http://rsbweb.nih.gov/ij).

Competitive and Noncompetitive Repopulation Assays. WT and *Vav1*$^{-/-}$ BM cells harvested from 5-fluorouracil-treated mice (150 mg/kg, i.v.) were transduced with retroviral vectors encoding EGFP and Venus, respectively (SF-IRES-GFP, SF-IRES-Venus) (5). Equal numbers of sorted $EGFP^+$ WT and $Venus^+$ *Vav1*$^{-/-}$ cells (3×10^5 cells per genotype and recipient) were mixed and transplanted into C57BL/10J mice together with 1×10^6 nontransduced C57BL/10J BM competitor cells. An independent experiment performed with the reverse color combination (Venus-WT and EGFP-*Vav1*$^{-/-}$) yielded similar results (data not shown). In additional competitive repopulation assays, freshly isolated WT or *Vav1*$^{-/-}$ BM cells (3×10^6 nucleated cells per recipient) were mixed with 3×10^6 B6.SJL cells and transplanted into B6.SJL mice. Recipients were bled monthly and killed 4 mo after transplant for the analysis of long-term BM and spleen engraftment; chimerism was assessed by flow cytometry.

For noncompetitive repopulation assays, WT or *Vav1*$^{-/-}$ BM cells (3×10^6 nucleated cells per recipient) were transplanted into B6.SJL recipients. Mice were monitored for survival and bled at different time points to assess peripheral blood counts.

Progenitor Homing Assays. Progenitor homing was measured essentially as described (2). Briefly, 1.5×10^7 WT or *Vav1*$^{-/-}$ nucleated BM cells were injected into lethally irradiated C57BL/10J mice. Femora were harvested 16 h posttransplant. Homing efficiency was calculated as the CFC frequency in recipient BM relative to that in the input BM sample. For the estimation of BM homing efficiency, it was assumed that one femur represents ~6% of the total BM content of the mouse (6).

Intravital Microscopy. HSPC microlocalization in the BM was analyzed by intravital microscopy using previously described equipment and procedures (7). Thirty thousand LSK cells were labeled with 1,1′-dioctadecyl-3,3,3′,3′-tetramethylindodicarbocyanine perchlorate (DiD) (Invitrogen) and injected into Nestin-GFP (8) or Col2.3-GFP (9) transgenic mice. A defined region of calvarium BM cavity (4 × 6 mm) was scanned using a confocal/two-photon hybrid microscope as previously described (7), allowing visualization of DiD^+ HSPC, $EGFP^+$ mesenchymal stem cells (MSC), or osteoblastic cells and endosteal matrix (collagen visualized by second-harmonic generation microscopy). Imaging was performed at 1 and 48 h posttransplant; three to five recipient mice were analyzed per recipient strain, time point, and genotype. For each DiD^+ cell identified, a Z stack was acquired. Distances were measured manually for each image in the Z stack, using ImageJ software (http://rsbweb.nih.gov/ij), and the shortest 3D distance was calculated. Cells were imaged at two time points posttransplant, 1 h (to determine the initial homing and localization) and 48 h (to assess short-term retention and the effect of proliferation as determined by clusters of DiD^+ cells with generally reduced dye intensity). Three to five recipient mice were analyzed per strain, time point, and donor genotype.

Statistical Analysis. Datasets were compared by two-tailed *t* tests; *P* values less than 0.05 were considered statistically significant.

1. Turner M, et al. (1997) A requirement for the Rho-family GTP exchange factor Vav in positive and negative selection of thymocytes. *Immunity* 7:451–460.
2. Cancelas JA, et al. (2005) Rac GTPases differentially integrate signals regulating hematopoietic stem cell localization. *Nat Med* 11:886–891.
3. Ploemacher RE, van der Sluijs JP, Voerman JS, Brons NH (1989) An in vitro limiting-dilution assay of long-term repopulating hematopoietic stem cells in the mouse. *Blood* 74:2755–2763.
4. Gu Y, et al. (2003) Hematopoietic cell regulation by Rac1 and Rac2 guanosine triphosphatases. *Science* 302:445–449.
5. Schambach A, et al. (2006) Equal potency of gammaretroviral and lentiviral SIN vectors for expression of O6-methylguanine-DNA methyltransferase in hematopoietic cells. *Mol Ther* 13:391–400.
6. Chervenick PA, Boggs DR, Marsh JC, Cartwright GE, Wintrobe MM (1968) Quantitative studies of blood and bone marrow neutrophils in normal mice. *Am J Physiol* 215:353–360.
7. Lo Celso C, et al. (2009) Live-animal tracking of individual haematopoietic stem/progenitor cells in their niche. *Nature* 457:92–96.
8. Mignone JL, Kukekov V, Chiang AS, Steindler D, Enikolopov G (2004) Neural stem and progenitor cells in nestin-GFP transgenic mice. *J Comp Neurol* 469:311–324.
9. Kalajzic Z, et al. (2002) Directing the expression of a green fluorescent protein transgene in differentiated osteoblasts: Comparison between rat type I collagen and rat osteocalcin promoters. *Bone* 31:654–660.

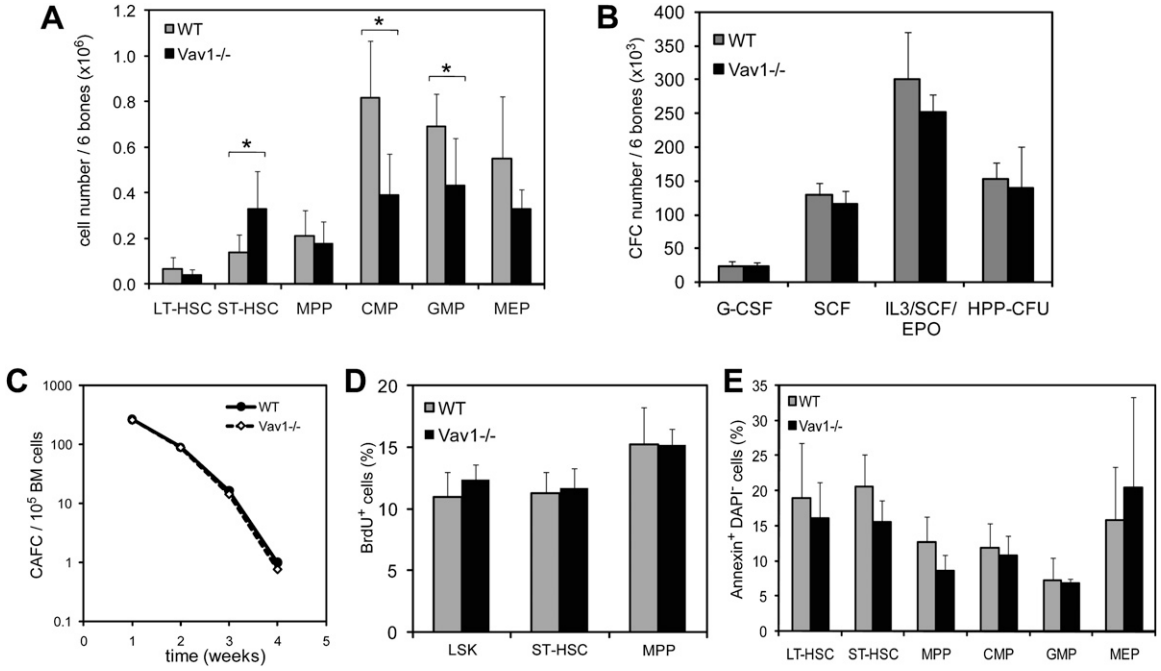

Fig. S1. Characterization of primitive hematopoietic cell populations in *Vav1*$^{-/-}$ mice. (*A*) Cell numbers (×10^6) in immunophenotypically defined HSPC subsets in the BM of WT and *Vav1*$^{-/-}$ mice, as determined by multiparameter flow cytometry. Cell populations were defined as explained in *Methods*. Data represent mean ± SD, $n = 7$, $^*P < 0.05$ (*t* test). (*B*) Number (×10^3) of CFC in the BM of WT and *Vav1*$^{-/-}$ mice obtained in the presence of single or multiple cytokines; $n = 7$ (HPP-CFU), $n = 4$ (all others). (*C*) Frequency of CAFC in WT or *Vav1*$^{-/-}$ BM. The *x* axis represents weeks in culture; the *y* axis represents the number of CAFC per 100,000 BM cells at each time point, determined by limiting dilution. (*D*) Fraction of BM cells in S phase after a 4-h pulse of BrdU in WT and *Vav1*$^{-/-}$ mice ($n = 4$). Cells were gated on immunophenotypically defined subsets. (*E*) Fraction of apoptotic (Annexin V$^+$ DAPI$^-$) cells in immunophenotypically defined HSPC subsets in the BM of WT and *Vav1*$^{-/-}$ mice ($n = 4$). LT, long-term; ST, short-term; CMP, common myeloid progenitors; GMP, granulocytic-monocytic progenitors; MEP, megakaryocytic-erythroid progenitors; MPP, multipotential progenitors.

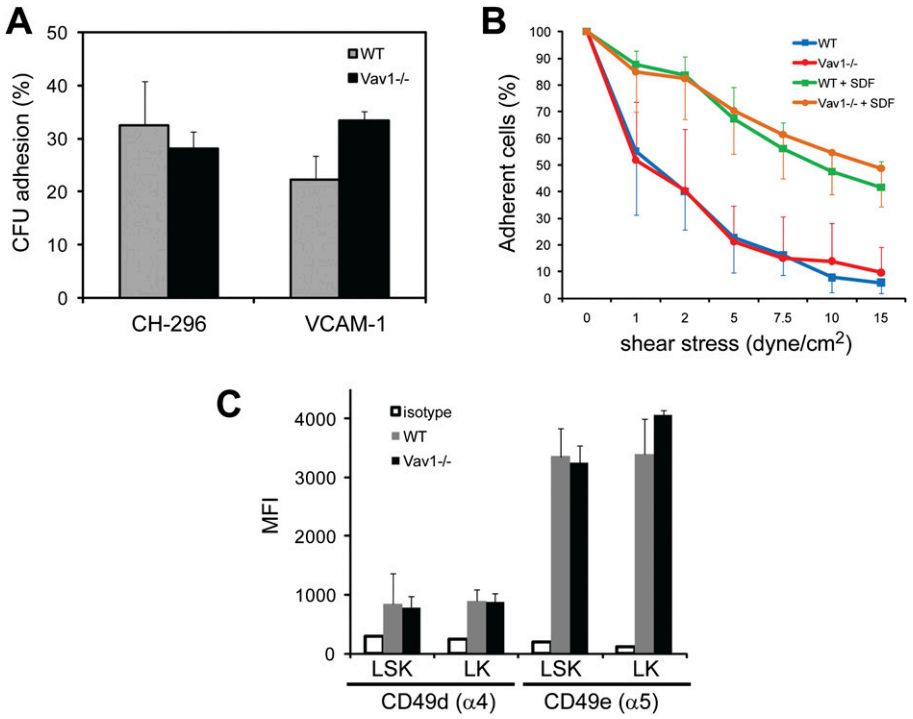

Fig. S2. Normal β_1 integrin-mediated adhesion of *Vav1*$^{-/-}$ progenitors. (*A*) Adhesion of WT or *Vav1*$^{-/-}$ progenitors to fibronectin (CH296)- or VCAM1-coated plates, expressed as the percentage of input CFC that stably adhered to the plate in 1 h. Data represent mean ± SD of triplicate wells. Shown is one representative experiment of a total of three that yielded similar results. (*B*) Firm adhesion of WT and *Vav1*$^{-/-}$ lin$^-$ c-kit$^+$ cells to VCAM1-coated microcapillaries under conditions of shear stress, expressed as the percentage of input cells that remain attached to the substrate after application of increasing flow rates. Each value of shear stress force, as indicated in the graph, was applied for 1 min. Data represent mean ± SD, n = 3–7. (*C*) Membrane expression of CD49d (α4) and CD49e (α5) integrin subunits in lin$^-$ Sca-1$^+$ c-kit$^+$ (LSK) or lin$^-$ Sca-1$^-$ c-kit$^+$ (LK) cells, determined by flow cytometry of WT and *Vav1*$^{-/-}$ BM cells. MFI, mean fluorescence intensity. n = 4 mice per genotype.

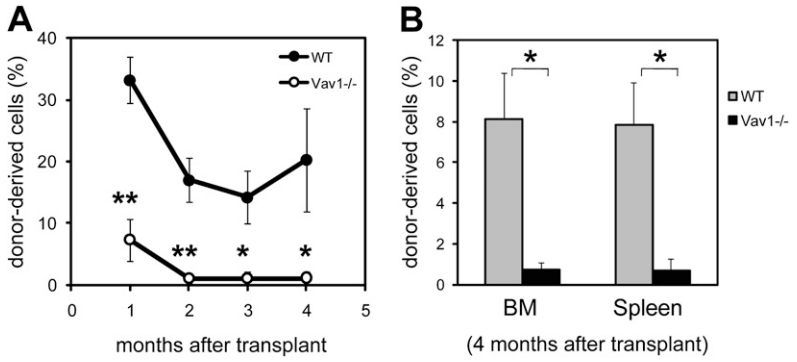

Fig. S3. Engraftment defect of *Vav1*$^{-/-}$ BM cells. (*A*) Peripheral blood chimerism of lethally irradiated C57BL/10J mice transplanted with 3×10^5 WT (EGFP$^+$), 3×10^5 *Vav1*$^{-/-}$ (Venus$^+$), and 1×10^6 nontransduced WT BM cells. (*B*) Chimerism in BM and spleen for the recipient mice in *A*, killed 4 mo after transplant. Data represent the percentage of EGFP$^+$ (WT) and Venus$^+$ (*Vav1*$^{-/-}$) cells in the nucleated fractions, determined by flow cytometry. Mean ± SD; n = 7, *$P < 0.01$, **$P < 0.001$ (t test).

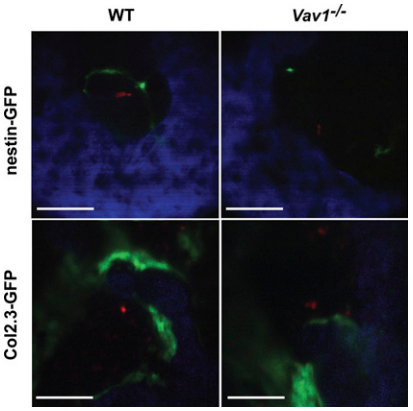

Fig. S4. Analysis of HSPC localization by intravital microscopy. Representative images of DiD-labeled WT or *Vav1*$^{-/-}$ LSK cells 1 h after transplant into Nestin-GFP or Col2.3-GFP mice, obtained by in vivo microscopy. Red, DiD (LSK cells); green, EGFP [nestin^{+} MSC (*Upper*) or osteoblastic cells (*Lower*)]; blue, bone (collagen visualized by second-harmonic generation microscopy). Microscopic fields are 330 × 330 μm. (Scale bars, 100 μm.)

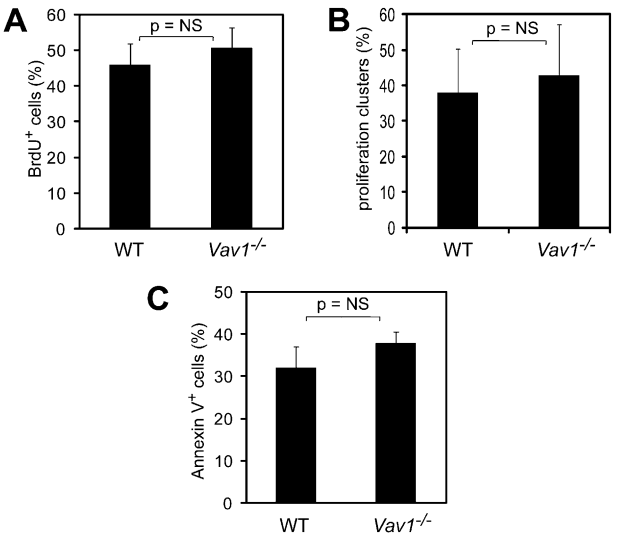

Fig. S5. Analysis of proliferation and apoptosis of transplanted HSPC. (*A*) Fraction of WT or *Vav1*$^{-/-}$ lin^{-} c-kit^{+} cells incorporating BrdU in the BM of lethally irradiated B6.SJL recipients. A 12-h BrdU pulse was given 48 h after transplant as described in *Methods*. Cells were gated on CD45.2 (donor-derived). Mean ± SD, n = 5–6. NS, nonsignificant. (*B*) Fraction of clusters of ≥2 DiD^{+} LSK cells 48 h after transplant observed by intravital microscopy. Mean ± SD, n = 3–4 recipients per genotype. (*C*) Fraction of WT or *Vav1*$^{-/-}$ CD45.2^{+} lin^{-} c-kit^{+} cells that were Annexin V^{+} 48 h after transplant into irradiated CD45.1 recipients. Mean ± SD, n = 3–4.

Table S1. Engraftment defect of *Vav1*$^{-/-}$ HSPC: Lineage reconstitution

		Peripheral blood [time after transplant (mo)]			
		1	4	Bone marrow	Spleen
CD11b^{+}	WT	15.68 ± 0.42	11.16 ± 4.37	40.50 ± 22.85	2.05 ± 1.28
	Vav1$^{-/-}$	3.23 ± 0.94	0.022 ± 0.032	0.14 ± 0.20	0.021 ± 0.031
B220^{+}	WT	35.93 ± 0.64	35.51 ± 13.71	13.94 ± 5.55	42.49 ± 10.57
	Vav1$^{-/-}$	4.14 ± 1.41	0.10 ± 0.16	0.56 ± 0.69	0.32 ± 0.32
CD3^{+}	WT	0.57 ± 0.65	2.80 ± 0.53	0.82 ± 0.20	6.49 ± 3.11
	Vav1$^{-/-}$	0.006 ± 0.014	0.010 ± 0.013	0.04 ± 0.07	0.067 ± 0.082

Lineage reconstitution at 1 and 4 mo, for the competitive transplant shown in Fig. 3 *A* and *B*, expressed as percentage of CD45.2^{+} cells relative to all viable white blood cells. Shown are data for myeloid (CD11b^{+}), B-lymphoid (B220^{+}), and T-lymphoid (CD3^{+}) lineages. Bone marrow and spleen were analyzed 4 mo posttransplant. Data represent mean ± SD, n = 5; $P < 0.05$ for all WT versus *Vav1*$^{-/-}$ comparisons.

Table S2. Engraftment defect of *Vav1*$^{-/-}$ HSPC: Lineage reconstitution

		Peripheral blood [time after transplant (mo)]					
		1	2	3	4	Bone marrow	Spleen
CD11b^{+}	WT	6.00 ± 2.59	4.73 ± 2.73	3.74 ± 1.99	4.72 ± 1.24	3.88 ± 2.06	0.47 ± 0.16
	Vav1$^{-/-}$	1.17 ± 0.44	0.23 ± 0.29	0.18 ± 0.18	0.23 ± 0.17	0.34 ± 0.17	0.09 ± 0.05
B220^{+}	WT	25.56 ± 2.48	10.75 ± 1.56	9.01 ± 2.43	11.54 ± 6.11	1.94 ± 0.36	4.47 ± 0.96
	Vav1$^{-/-}$	5.69 ± 2.91	0.80 ± 0.48	0.86 ± 0.90	0.80 ± 0.85	0.27 ± 0.25	0.54 ± 0.50
CD3^{+}	WT		1.57 ± 0.32	1.46 ± 0.27	2.58 ± 1.24	0.57 ± 0.43	2.32 ± 1.13
	Vav1$^{-/-}$		0.04 ± 0.04	0.04 ± 0.02	0.10 ± 0.05	0.13 ± 0.04	0.17 ± 0.07

Lineage reconstitution at 1–4 mo, for the competitive transplant shown in Fig. S3, expressed as percentage of EGFP+ (WT) or Venus+ (*Vav1*$^{-/-}$) cells, relative to all viable white blood cells. Shown are data for myeloid (CD11b+), B-lymphoid (B220+), and T-lymphoid (CD3+) lineages. Bone marrow and spleen were analyzed 4 mo posttransplant. Data represent mean ± SD, n = 5–7; $P < 0.05$ for all WT versus *Vav1*$^{-/-}$ comparisons.

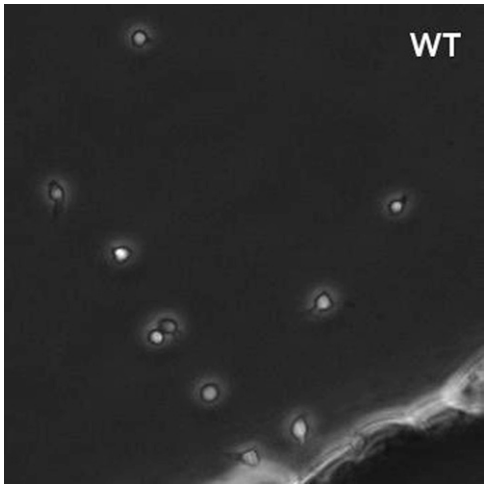

Movie S1. Migration of WT LSK cells adhered on a fibronectin-coated coverslip, subjected to an SDF1α gradient in a Dunn chemotaxis chamber and imaged by time-lapse microscopy (2 frames/min for 1 h). Field dimensions are 227.5 × 227.5 μm.

Movie S1

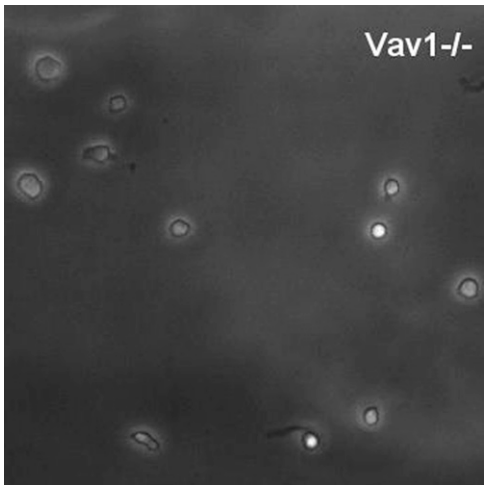

Movie S2. Migration of *Vav1*$^{-/-}$ LSK cells adhered on a fibronectin-coated coverslip, subjected to an SDF1α gradient in a Dunn chemotaxis chamber and imaged by time-lapse microscopy (2 frames/min for 1 h). Field dimensions are 227.5 × 227.5 μm.

Movie S2